Published in: Journal of Applied Physics https://aip.scitation.org/journal/jap
Volume: 124 **Issue:** 10 **Article Number:** 105304 **DOI:** 10.1063/1.5030049 **Published:** SEP 14 2018

For personal use only

Influence of the thickness of a nanometric copper interlayer on Au/dielectric thermal boundary conductance

Maïté Blank and Ludger Weber

Laboratoire de Métallurgie Mécanique, Ecole Polytechnique Fédérale de Lausanne, Lausanne, Switzerland

ABSTRACT

The influence of the thickness of a thin (1.5 - 30 nm) copper layer on the thermal boundary conductance (TBC) at the interface between gold and silicon, sapphire and diamond, respectively, was studied by Time Domain Thermoreflectance (TDTR). Overall, a monotonic increase of the TBC was observed over the first 10 nm, before reaching a plateau. In some cases, it was also observed that an interlayer reduced the TBC as compared to the reference system. This is rationalized by assuming that the TBC evolution as a function of the interlayer thickness is controlled by i) a contribution of the gold layer that has to be taken into account for all phonons having a wavelength larger than the interlayer thickness and ii) a thickness-dependant resistance within the interlayer that appears when electron-phonon coupling is incomplete, i.e. typically over the first 10 nm. A model is proposed in which the contribution to thermal boundary conductance by phonons coming directly from the gold layer is estimated using a simple Debye approximation, while the resistance that appears within the interlayer is estimated by $g(T)$ times h with $g(T)$ the electron-phonon coupling factor and h the interlayer thickness. This results in a system with three resistances in series, i.e. the metal-metal and metal-dielectric interfacial resistances and the interlayer resistance, and a contribution due to phonons the gold layer. Reasonably good agreement between this model and experimental data is observed.

I. INTRODUCTION

The recent evolution of electronic devices towards micro- and nano-scale raises new challenges in the field of thermal management. In particular, engineering of interfaces becomes essential because they are the major barriers to efficient heat transport in many applications such as dot lasers (1), heat-assisted magnetic recording diodes (2) or vertical cavity surface emitting lasers (3). In solid-solid systems, metal-dielectric and dielectric-dielectric interfaces are much more critical than interfaces with electron conductors on both sides. The latter exhibit a thermal boundary conductance (TBC) typically above 500

MW/m^2K, whereas the former can be as low as 10 MW/m^2K, e.g. Bi/diamond (4). Assuming diamond thermal conductivity to be 2000 W/mK, this corresponds to a Kapitza length of 200 µm. In an attempt to improve TBC, extensive studies have been carried out and highlighted that metal irradiance (5), materials elastic mismatch (4), and interfacial bonding (6–8) are key parameters to take into account. Insertion of a thin interlayer that reduces interfacial mismatch was also discussed in several contributions. Schmidt *et al*. (9) showed that the insertion of a thin Ti interlayer at the interface between Al and graphite enhances TBC by a factor of 2, reaching values close to those obtained at the Ti/graphite system. The authors concluded that under such a configuration, the Ti layer was controlling thermal transport and that TBC improvement could be attributed to a stronger interfacial bonding. Similar features have been observed by Duda *et al*. (10) on Au/Si interfaces by adding a thin Ti adhesion layer. Wang and Cahill (11) studied Al and Pt interlayers ranging from 10 to 100 nm inserted at Au/Si interfaces. They linked the observed improvements of TBC to an increase of the electron-phonon coupling constant g within the interlayer (g = $2.5x10^{17}$, $10.8x10^{17}$ and $0.26x10^{17}$ MW/m^3K for Al, Pt, and Au, respectively). The evolution of the conductance for ultra-thin interlayers (< 10 nm) was however not explored in their work. Jeong *et al*. (12) attempted to fill this gap by studying the influence of both copper and chromium interlayers ranging from 0 to 8 nm inserted at Au/Al_2O_3 interfaces on TBC. They observed a monotonic increase of TBC as a function of the interlayer thickness. This evolution was explained using a modified diffuse mismatch model (DMM) and assuming that the adhesion layer contributes to the thermal transport only when its thickness is larger than the phonon wavelength. A possible effect of change in electron-phonon coupling factor was however not considered.

In an attempt to tackle a possible role of the electron-phonon coupling factor and with the aim of deepening our understanding of the mechanisms involved in thermal transport at the interface between a metal and a dielectric when an nm-sized adhesion layer is added, the effect of copper layers ranging from 1.5 to 30 nm on TBC on Au/Si, Au/Al_2O_3, and Au/diamond interfaces is investigated here. The results indicate that the electron-phonon coupling factor is indeed important in the evolution of TBC with nm-sized interlayers. It is shown that an adapted version of a model based on the work of Wang and Cahill (11) that takes into account the evolution of the electron-phonon coupling contribution as the interlayer thickness increases, coupled with a phonon tunnelling effect, fits well our experimental data. A schematic sketch of the heat transport mechanisms involved in such a configuration is given in Figure 1, resulting in resistances acting either in series (metal/metal and interlayer/dielectric interfacial resistance, as well as the electron-phonon coupling resistance) or in parallel (resistance related to a metal/dielectric transparency effect).

II. EXPERIMENTAL

a. Sample preparation and characterization

Cr-Au-Cu stacks were deposited on silicon, sapphire and diamond using an Alliance-Concept DP650 sputtering machine. The chromium top layer served as a transducer and was about 20 nm thick. The gold layer was set to 80 nm approximately and the thickness of the copper interlayer was varied from 1.5 to 30 nm. Cr-Au and Cr-Cu stacks were also produced for all substrates to serve as a reference. Samples were kept under vacuum during the whole stack

deposition process. Prior to deposition, all [100] Si wafers were RCA cleaned. HF-dip in a 1% HF aqueous solution was further performed right before placing the wafer in the deposition unit to remove surface native oxide. c-plane [0001] Al_2O_3 (Ref. 2561 purchased from UniversityWafer) wafers were cleaned using successively acetone, ethanol and isopropanol in an ultrasonic bath. Potential organic contamination was removed right before deposition with a 15 min Ar:O plasma treatment performed in a Fischione 1020 plasma cleaner, using a gas mixture of Ar:O_2 3:1. Diamond stones (Ref. MWS L25 with [100] oriented surfaces purchased from Element 6, Shannon, Co. Clare, Ireland) were prepared in a similar way as previously described (13). Each diamond was first polished using 6, 3 and 1 µm diamond paste and olive oil as a lubricant. Fine polishing was achieved using 1 µm diamond paste and a mixture of water, ethanol and soap as a lubricant. Surface reactivity was finally induced right before deposition by performing a 15 min Ar:O plasma treatment similar to the one described above.

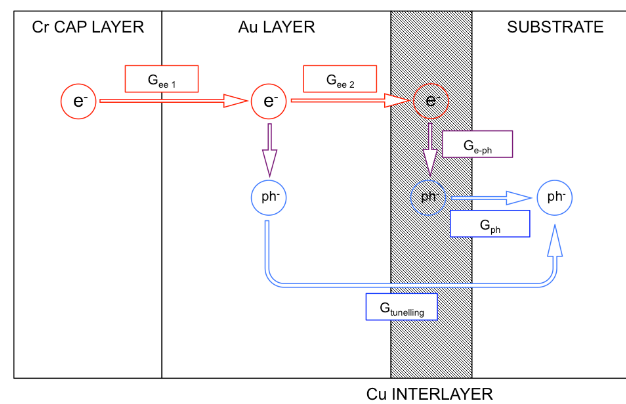

Fig. 1: Mechanisms involved in heat transfer at metal-dielectric interfaces with the addition of a thin interlayer.

Knowing that the thermal diffusivity of silicon, sapphire and diamond is $7.6 \cdot 10^{-5}$, $1.1 \cdot 10^{-5}$ and $6 \cdot 10^{-4}$ m^2/s, respectively, and that the maximum delay time achievable with our TDTR setup is 4 ns (see § II.b), the maximum achievable diffusion length is 0.5 µm for silicon, 0.2 µm for sapphire and 1.5 µm for diamond, which for all cases is much shorter than the sample thickness being, respectively, 525 µm, 600µm and 1mm.

The exact thickness of each layer was measured for all samples with X-Ray Reflectivity (XRR) using an XRD Empyrean Diffractometer and fitting the curves using the GenX software (14). Layers and substrate thickness, density and roughness as well as intermixing between two neighbouring layers were used as fitting parameters. Figure 2 shows typical experimental data and fitting curves obtained on Cr-Au-Cu/Si samples. The validity of the measurement technique was previously confirmed by TEM imaging on a set of calibration samples. Both techniques showed close agreement in derived layer thicknesses.

The uniformity of the interlayers was ensured using SEM imaging (Zeiss Merlin SEM) on silicon, sapphire and diamond samples covered by a 1.5 nm copper layer, which corresponds to the thinnest layer observed during this work. In all cases, the layer obtained was found to be continuous without any sign of island formation.

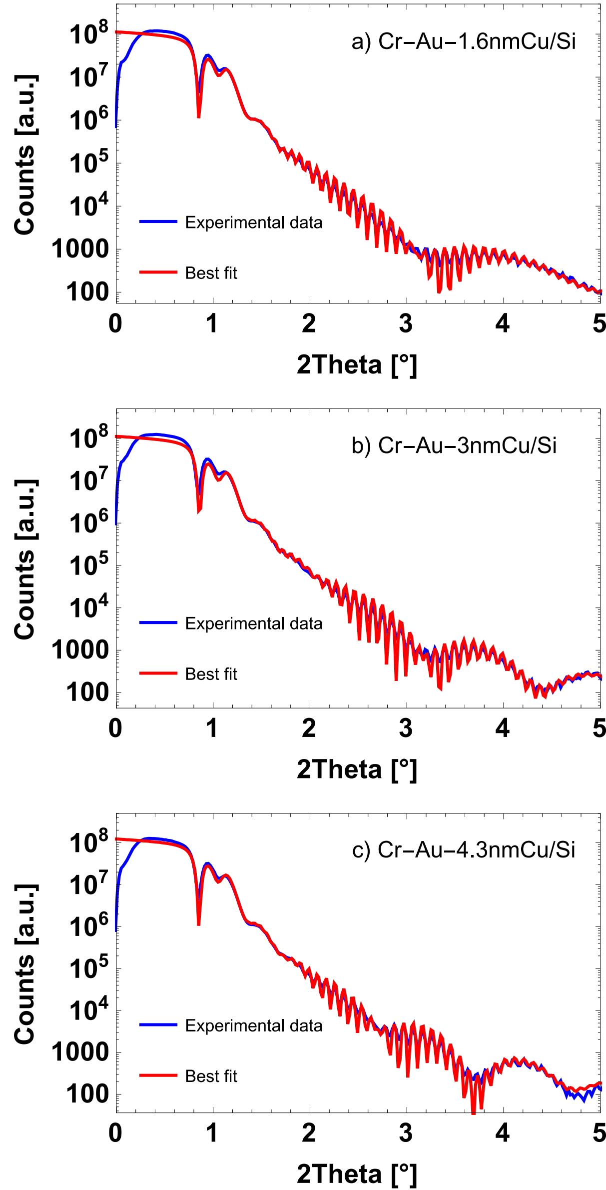

Fig. 2: X-Ray Reflectance (XRR) experimental data and fitting curves obtained for a) Cr-Au-1.6nmCu/Si, b) Cr-Au-3nmCu/Si, c) Cr-Au-4.3nmCu/Si. Changes occurring from 3 to 5° are directly related to Cu, indicating a high sensitivity to the interlayer thickness.

b. Thermal boundary conductance measurement

The thermal boundary conductance between the metallic stack and its substrate was measured using a Time Domain Thermoreflectance (TDTR) setup similar to the one described in detail previously (13,15). A Coherent Mira 900 laser having a repetition rate of 76 MHz and operating at 785 nm was used for this setup, which consists in separating the initial beam into a pump (that heats the sample periodically) and a probe (that monitors surface temperature through a change in reflectivity) that are focused on the same spot on the sample surface. The pump is modulated at 10.7 MHz using an Electro-Optic Modulator (EOM), while the reflected signal is monitored using a fast photodiode before being frequency filtered at this

same frequency, amplified and fed into a ZI HF2 digital lock-in amplifier. Most of the noise related to the pump is supressed using different polarizations and slightly separated “two tints” wavelengths for the two beams. Full curves were obtained using a delay stage that is mounted on the pump path and that enables sweeping a large range of delay times (0 - 4 ns).

All experiments were carried out using fluences of ~ 0.2 mJ/cm^2 and a 1/e^2 radius of approximately 4 μm. Although these values were relatively constant throughout all measurements, the exact values of beam power and spot size and thus the fluence were recorded for each single experiment using a laser power meter and a CMOS camera, respectively.

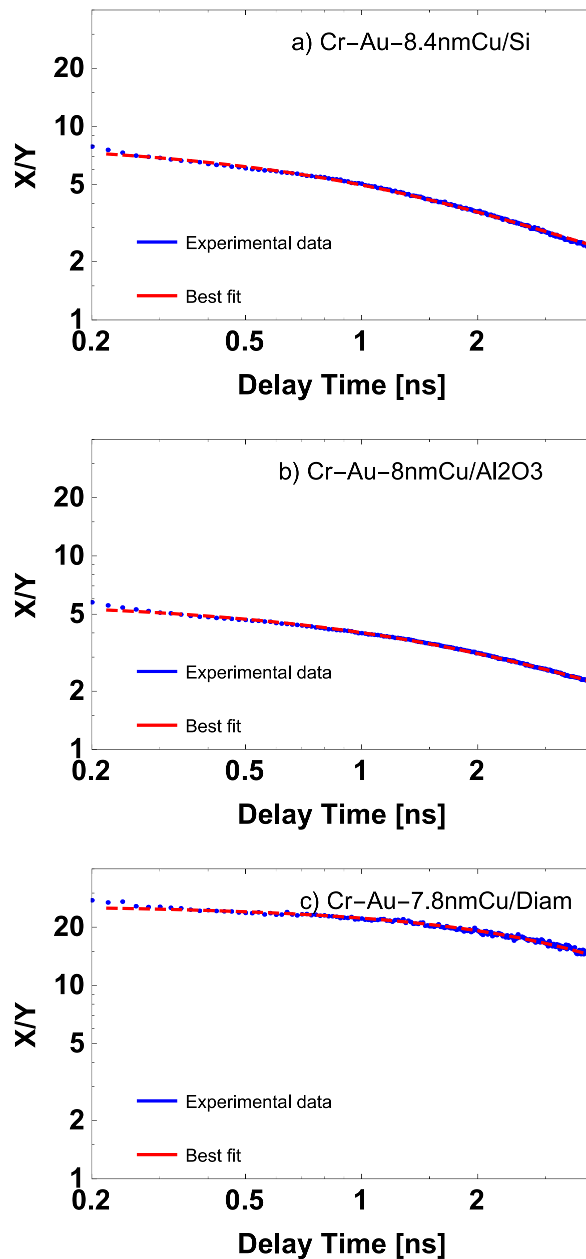

Fig. 3: Raw signal and fitting curve obtained for a) Cr-Au-7.8nmCu/Diam b) Cr-Au-8.4nmCu/Si c) Cr-Au-8nmCu/Al_2O_3.

The model proposed by Cahill (16) was used to extract TBC values, fitting the model to the X/Y ratio calculated from values obtained with the lock-in. The fitting parameters were TBC and substrate conductivity, while other values of thermal conductivity and heat capacity were taken from the literature (17). Metal-metal interfacial resistance at the Cr/Au interface was not taken into account for the X/Y signal analysis because it doesn't affect the end result, since the TDTR measurement is fairly insensitive to it. Examples of typical raw signals and fitting curves are given for each substrate in Figure 3. A good signal to noise ratio, as well as a satisfactory quality of the fits was obtained in all cases.

III. RESULTS

The thermal boundary conductance of Au on Si, Al_2O_3 and diamond was measured to be 126, 48, and 75 MW/m^2K, respectively, while the thermal boundary conductance of Cu on these substrates was found to be 347, 194, and 104 MW/m^2K. The typical experimental variability observed in a series of measurements on the same sample was below 7%, while the overall precision was evaluated to be uncertain to ±20%. The TBC values were in good agreement with those obtained by other groups (12,13,18–20) and were further used as reference points to characterize the influence of the copper interlayers.

Figure 4 and Figure 5 show the evolution of the TBC with increasing thickness of the copper interlayer at Au/Si and Au/Al_2O_3 interfaces. Already a Cu-interlayer as thin as 1.5 nm at the Au/Si interface improves TBC from 126 to 147 MW/m^2K. Over the first 10 nm the TBC increases monotonically up to 260 MW/m^2K, which is about twice the value obtained at the Au/Si interface alone and 75% of the value measured at the Cu/Si interface. For thicker layers, a plateau is reached with an average TBC value of 250 MW/m^2K. A qualitatively similar behaviour was obtained when adding copper interlayers at the Au/Al_2O_3 interface. The

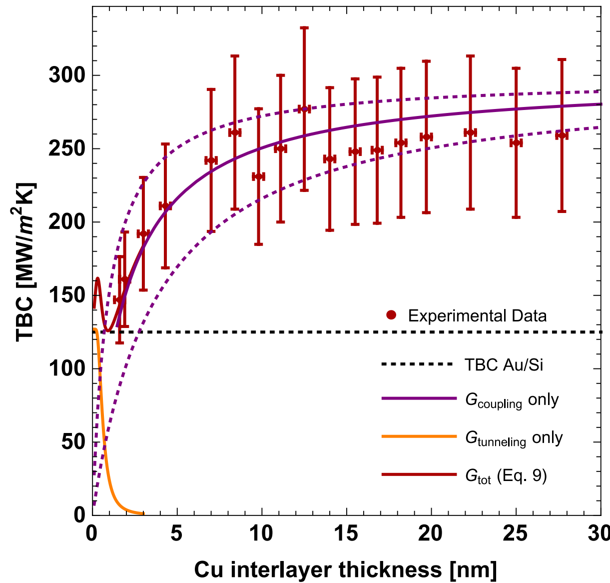

Fig. 4: Influence of the addition of a nm-sized copper interlayer on thermal boundary conductance at the Au/Si with i) $G_{coupling}$ obtained using Eqs. 1-3, in which $G_{e\text{-}ph}$ is assumed to evolve with the interlayer thickness. Dotted purple lines show the curves corresponding to $2 \cdot G_{e\text{-}ph}$ and $0.5 \cdot G_{e\text{-}ph}$ respectively, ii) $G_{tunnelling}$ obtained using Eqs. 6-8, in which gold contribution is assumed to decrease with increasing interlayer thickness, iii) G_{tot} obtained using Eq. 10, which combines both the electron-phonon coupling and the tunnelling effects.8nmCu/Al_2O_3.

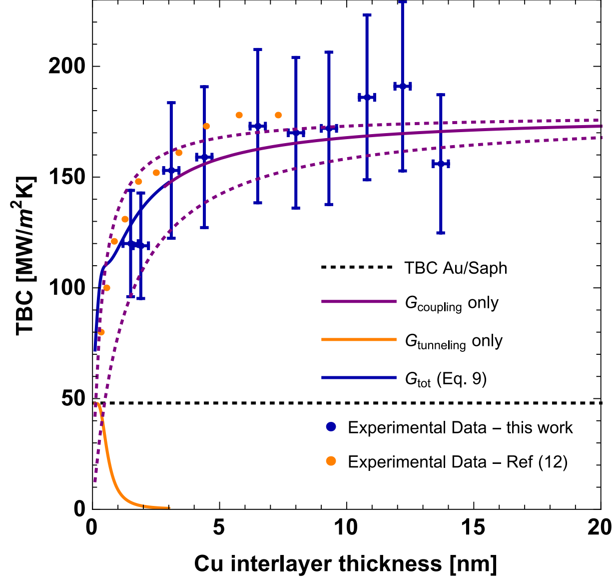

Fig. 5: Influence of the addition of a nm-sized copper interlayer at the Au/Al_2O_3 interface, comparison between the results obtained within this work and those published by Jeong *et al*. (12). i) $G_{coupling}$ obtained using Eqs. 1-3, in which G_{e-ph} is assumed to evolve with the interlayer thickness. Dotted purple lines show the curves corresponding to $2 \cdot G_{e-ph}$ and $0.5 \cdot G_{e-ph}$ respectively, ii) $G_{tunnelling}$ obtained using Eqs. 6-8, in which gold contribution is assumed to decrease with increasing interlayer thickness, iii) G_{tot} obtained using Eq. 10, which combines both the electron-phonon coupling and the tunnelling effects.

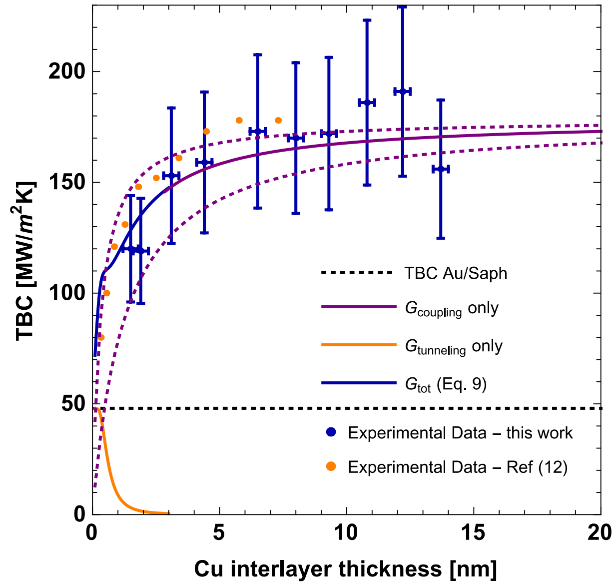

Fig. 6: Influence of the addition of a nm-sized copper interlayer on thermal boundary conductance at the Au/diamond interface. i) $G_{coupling}$ obtained using Eqs. 1-3, in which G_{e-ph} is assumed to evolve with the interlayer thickness. Dotted purple lines show the curves corresponding to $2 \cdot G_{e-ph}$ and $0.5 \cdot G_{e-ph}$ respectively, ii) $G_{tunnelling}$ obtained using Eqs. 6-8, in which gold contribution is assumed to decrease with increasing interlayer thickness, iii) G_{tot} obtained using Eq. 10, which combines both the electron-phonon coupling and the tunnelling effects.

TBC jumps from 48 to 120 MW/m^{2}K with the addition of a 1.5 nm interlayer, while a 8 nm interlayer allows reaching values as high as 169 MW/m^{2}K, i.e. more than threefold the value

measured for Au/Al_2O_3 and about 85% of the value measured at the Cu/Al_2O_3 interface. The plateau value was observed to be 175 MW/m^2K.

The results obtained for the Au/diamond are shown in Figure 6 and exhibit slightly different features as compared to the two other substrates. The TBC increases monotonically as a function of copper thickness, similarly to the Au/Si and Au/Al_2O_3 systems. Unlike the observation on Si and Al_2O_3 substrates, the addition of a copper interlayer on diamond thinner than 4 nm led to reduced TBC as compared to the value obtained for the reference sample. As an example, TBC was measured to be 64 MW/m^2K with a 3 nm copper interlayer, while it was 75 MW/m^2K without it. The plateau value was observed to be 85 MW/m^2K.

IV. DISCUSSION

a. Sensitivity

Interlayer thickness being one of the input parameters used while extracting TBC from TDTR measurements, the validity of TBC values was ensured by evaluating TDTR measurement sensitivity to interlayer thickness using Eq. 1.

$$S_{i(T)} = \frac{\partial \ln\left[-\frac{X(t,T)}{Y(t,T)}\right]}{\partial \ln[i(T)]} \qquad (1)$$

with i the parameter under consideration and S_i the TDTR measurement sensitivity to this parameter. An S_i value of 0 typically means that even large changes in parameter i won't affect TDTR measurement. While S_i value increases, TDTR measurement becomes more and more sensitive to parameter i, meaning that relative changes of this parameter will influence TDTR measurement with a strength that depends directly on S_i value.

$S_{\text{Cu thick}}$ was found to be very small for all interlayer thicknesses at all delay times and for all substrates (see Fig. 7) with maximum values never exceeding 0.2. This indicates that TBC evolution with interlayer thickness is a real physical phenomenon that is not due to a possible error in interlayer thickness measurement.

For all substrates, the evolution of thermal conductivities resulting from the evaluation procedure of TDTR measurements to derive TBC values was further analysed as a function of interlayer thickness. It can be seen from Fig. 8 that i) no correlation between the substrate thermal conductivity and the interlayer thickness could be identified, and ii) the thermal conductivities were found to be reasonably close to theoretical values. A relatively large variation in diamond thermal conductivity was observed but is not unusual given the strong influence the actual nitrogen content has on thermal conductivity and that this nitrogen content varies both from one diamond single crystal to another and within a large single crystal spending on whether the measurement point was taken on the seed part or the secondary growth part of the diamond. Both observations indicate that the TBC values are not very likely to be affected by an inappropriate bias coming from leaving the substrate thermal conductivity as a free parameter in TBC evaluation.

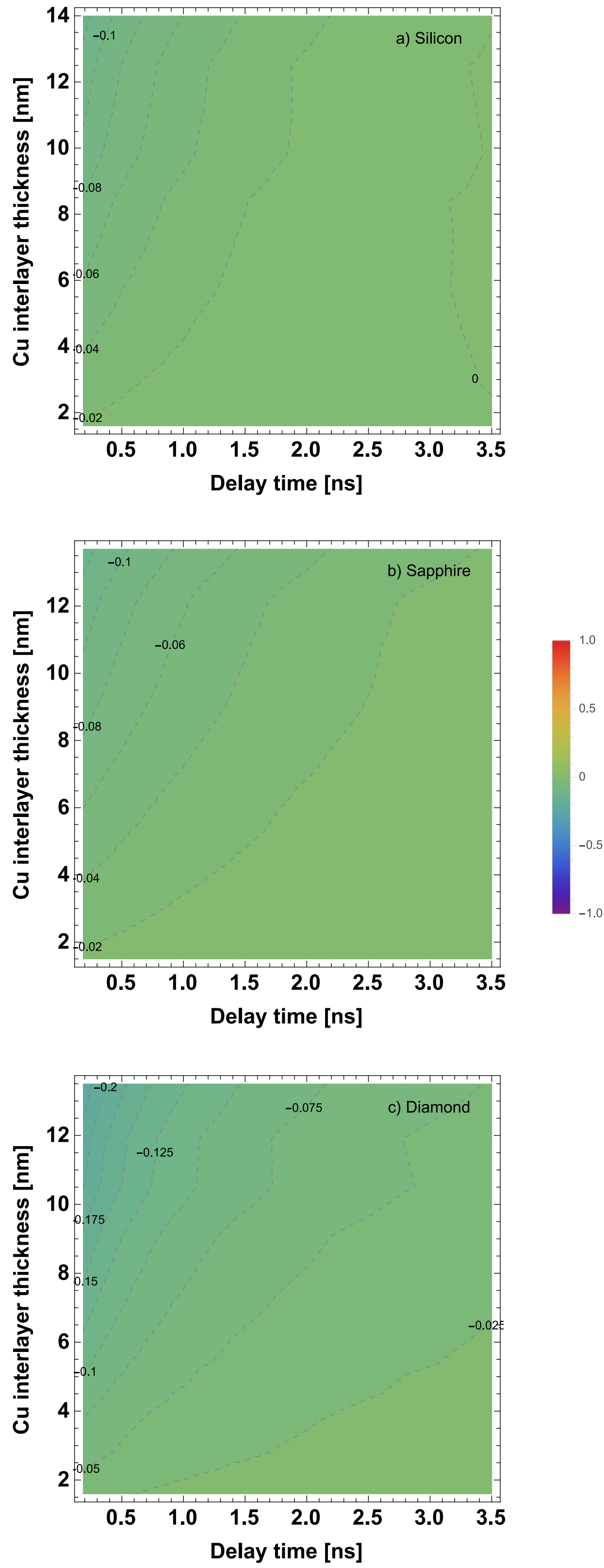

Fig. 7: TDTR measurement sensitivity to interlayer thickness on a) silicon, b) sapphire and c) diamond substrates.

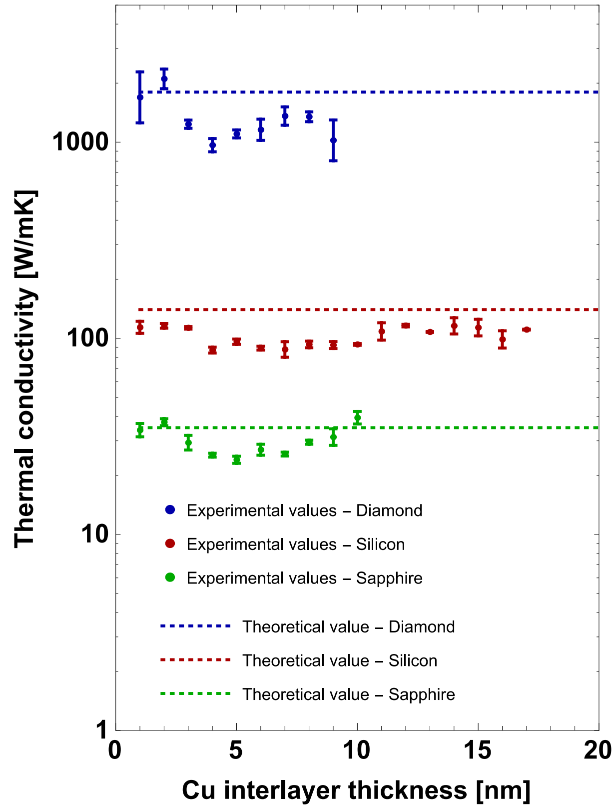

Fig. 8: Thermal conductivity measured as a function a Cu interlayer thickness for silicon, sapphire and diamond. Dashed lines indicate the theoretical value.

b. TBC evolution with Cu interlayer thickness

First, we observe that the experimental data obtained within this work for the Au-nm Cu/sapphire system are in rather good agreement with those obtained by Jeong et al. (12) (cf. Figure 5) giving us confidence that our procedures are sound. Combining the results obtained on the three different substrates, we observe two consistent features: i) the increase in TBC occurs over a relatively constant range of thicknesses (over the first 10 nm) before reaching a plateau and ii) in some cases, TBC can fall below the values of the reference sample.

Both findings are at odds with the interpretation proposed by Jeong et al. (12) who rationalized the observed evolution with layer thickness by phonon transparency, i.e. the transfer of phonons with a wavelength larger than the interlayer thickness being controlled by the phonon DOS of gold, while those with a wavelength shorter than the interlayer thickness being controlled by the phonon DOS of copper (the interlayer material). For such a physical mechanism, the TBC should reach the plateau value to within a few per cent at interlayer thickness on the order of 1 - 2 nm and should show a continuous transition from a TBC characteristic of the layer/substrate couple to the one of the interlayer/substrate couple.

The alternative mechanism based on electron-phonon coupling proposed by Wang and Cahill (11) is not satisfactory either since for very small thicknesses the theory by Wang and Cahill leads to a TBC approaching zero. We hence suggest that both mechanisms are relevant and

develop in what follows the resulting expression for the TBC in a system with a metallic interlayer.

In metals, the electron-phonon coupling parameter $g(T)$ describes the exchange of thermal energy between electrons and phonons per unit volume. This parameter is negligible in systems where layers are thick enough to allow full thermalisation. It can however significantly contribute to thermal resistance in systems where ultra-thin layers are present. As suggested by Wang and Cahill (11), a full description of this phenomena is made easier by defining an effective thermal conductance per unit area that is given by the product of $g(T)$ and the layer thickness h. As shown in Figure 1, the thermal resistance $1/hg(T)$ acts in series with the metal-metal interfacial resistances $1/G_{ee,1}$ (Cr-Au) and $1/G_{ee,2}$ (Au-Cu) and with the metal-dielectric interfacial conductance G_{ph}. The total thermal resistance $1/G_{coupling}$ can thus be expressed using Eq. 2 and 3:

$$\frac{1}{G_{\mathrm{coupling}}} = \frac{1}{G_{\mathrm{e-ph}}} + \frac{1}{G_{\mathrm{ph}}} \qquad (2)$$

$$G_{\mathrm{e-ph}} = \frac{G_{\mathrm{ee,1}} G_{\mathrm{ee,2}} hg(T)}{G_{\mathrm{ee,1}} G_{\mathrm{ee,2}} + G_{\mathrm{ee,1}} hg(T) + G_{\mathrm{ee,2}} hg(T)} \qquad (3)$$

G_{ee} can be estimated using Eq. 4 (21):

$$G_{\mathrm{ee}} = \frac{Z_{\mathrm{el,1}} Z_{\mathrm{el,2}}}{4(Z_{\mathrm{el,1}} + Z_{\mathrm{el,2}})} = \frac{\gamma_{\mathrm{s,1}} v_{\mathrm{s,1}} \gamma_{\mathrm{s,2}} v_{\mathrm{s,2}}}{4(\gamma_{\mathrm{s,1}} v_{\mathrm{s,1}} + \gamma_{\mathrm{s,2}} v_{\mathrm{s,2}})} T \qquad (4)$$

with $Z_{el,i} = \gamma_{s,i} v_{s,i} T$, with $\gamma_{s,i}$ is the Sommerfeld parameter that characterizes the electronic heat capacity and $v_{s,i}$ is the Fermi velocity.

Table I summarizes the values used in this work. All Sommerfeld constants were taken from Kittel (22), while all Fermi velocities were calculated using the number of electrons per unit volume from (17).

Table I : Cr, Au and Cu Sommerfeld coefficient and Fermi velocity used to calculate the electronic thermal boundary conductance G_{ee}.

Metal couple	$\gamma_{s,1}$ [J/m^{3}K]	$v_{s,1}$ $\cdot 10^6$ [m/s]	$\gamma_{s,2}$ [J/m^{3}K]	$v_{s,2}$ $\cdot 10^6$ [m/s]	G_{ee} [GW/m^{2}K]
Cr-Au	193.6	2.84	71.5	1.39	4.9
Au-Cu	71.5	1.39	98.1	1.57	4.5

Comparing our experimental data to the model described by Eq. 2-4 requires knowledge of the electron-phonon coupling factor, which is not easy to determine. For copper, Hohlfeld *et al*. (23) and Wang and Cahill (11) found 1x10^{17} and 0.75x10^{17} MW/m^{3}K, respectively. Lin (24) however suggested that this value is strongly dependant on the electron temperature in the system. Therefore, *g(T)* was taken as a free parameter in fitting Eq. 2 to our experimental

data using a quasi-Newton method implemented in Mathemetica. G_{ph} and G_{tot} were taken from our experimental data and G_{ee} calculated from Eq. 4. As a results, we found $g(T)_{Cu,Si} = 1.51 \times 10^{17} \pm 0.3 \times 10^{17}$ MW/m^{3}K, $g(T)_{Cu,sapphire} = 2.71 \times 10^{17} \pm 1.1 \times 10^{17}$ MW/m^{3}K, $g(T)_{Cu,diamond} = 0.66 \times 10^{17} \pm 0.2 \times 10^{17}$ MW/m^{3}K. The variability of these values is attributed to the fact that TBC evolution has a strong influence on $g(T)$, while the experimental data are precise to 20% only. They remain however close to each other and in good general agreement with the values obtained by Hohlfeld *et al.* (23) and Wang and Cahill [11]. The precision obtained on $G_{e\text{-}ph}$ measurement is indeed sufficient to provide a qualitative description of the mechanisms involves. As shown in Figs. 4-6, changing $G_{e\text{-}ph}$ the overall tendency remains the same, although quantitatively affecting the fit. In particular, it captures well TBC evolution with interlayer thickness occurring over a dozen of nanometers.

A phonon transparency effect was further added and evaluated using the thermal transport equation under the Debye approximation (Eq. 5).

$$G_{tunelling}(\omega) = \frac{1}{2} \sum_p \int_0^{\pi/2} \int_0^{\omega_{max}} \hbar \omega v(p) \frac{\partial n(\omega, T)}{\partial T} \frac{\omega^2}{2\pi v^3(p)} \alpha_{1\to 2} \sin\theta \cos\theta \, d\theta d\omega \qquad (5)$$

with p, ω and θ the phonon polarization, frequency and incidence angle respectively, v the sound velocity, θ_D the Debye temperature, $n(\omega,T)$ the Planck distribution function and $\alpha_{1\to 2}$ the phonon transmission coefficient, where the subscripts 1 and 2 represent the materials having the lowest and the highest Debye temperature respectively.
Getting an expression that depends on phonon wavelength λ is then possible through the variable change expressed by Eq. 6.

$$\omega = 2\pi \frac{v(p)}{\lambda} \qquad (6)$$

Combining Eqs. 5 and 6 yields:

$$G_{tunnelling}(\lambda) = \sum_p \int_0^{\frac{\pi}{2}} \int_{\lambda_{\min} = \frac{v_{av}}{\omega_{\max}}}^{\infty} C(p,\theta) \frac{e^{\frac{k}{\lambda}}}{\left(e^{\frac{k}{\lambda}} - 1\right)^2 \lambda^6} \, d\lambda \, d\theta \quad (7)$$

with $C(p,\theta)$ and k two fitting parameters.

These fitting parameters were determined assuming that i) integrating Eq. 7 over all possible wavelengths gives the experimental TBC value observed at the Au/substrate interface (Eq. 8) and that ii) the maximum of the function given in Eq. 7 is located at $\lambda = 2\pi v_{av}/\omega_{max}$, which corresponds to the lowest wavelength observed in the DOS as described by Debye model (Eq. 9).

$$\int_0^{\infty} C(p,\theta) \frac{e^{\frac{k}{\lambda}}}{\left(e^{\frac{k}{\lambda}} - 1\right)^2 \lambda^6} d\lambda = G_{\text{ph Au,substrate}} \qquad (8)$$

$$\left.\frac{d\left(C(p,\theta)\frac{e^{\frac{k}{\lambda}}}{\left(e^{\frac{k}{\lambda}}-1\right)^{2}\lambda^{6}}\right)}{d\lambda}\right|_{\lambda=\frac{2\pi v_{\mathrm{av}}}{\omega_{\mathrm{max}}}}=0 \qquad (9)$$

with $\omega_{\max}$ the maximum phonon frequency and v_{av} the average sound velocity in the metal under consideration. For gold, these values were found to be 4.7 THz (25) and 2153 m/s (26) respectively. As a result, we obtained *C(p,θ)* = 763, 281, and 442 for silicon, sapphire, and diamond, respectively, while *k* equaled 2.73 for all substrates.

A simple parallel resistance model is adopted to take into account both, the influence of the electron-phonon coupling factor, and the gold layer contribution as expressed by Eq. 10

$$G_{tot} = G_{coupling} + G_{tunnelling}(\lambda) \qquad (10)$$

Figure 4 to Figure 6 show the fits obtained using the aforementioned parameters *g(T), C(p,θ)* and *k*. As a result, we observe a good agreement between the experimental data and the model. The initial increase of TBC observed for G_{tot} is an artefact that is attributed to the simplifications made within Debye model. This model catches all the important features observed by the experiments, suggesting that it captures the main mechanisms involved in TBC evolution when a thin interlayer is added between a metal and a dielectric.

V. CONCLUSION

The effect of a thin (1.5 – 30 nm) copper layer on the TBC at Au/Si, Au/Al_2O_3 and Au/diamond interfaces was studied. It was observed that TBC increases monotonically over the first 10 nm before reaching a plateau. Furthermore, in the case of diamond, very thin interlayers ranging from 1.5 to 4 nm would reduce TBC as compared to the one measured for Au/diamond alone. Based on these features, we suggest that a tunnelling effect, in which the phonons are either governed by gold or copper properties depending on their wavelength and the interlayer thickness, is not sufficient to explain the observations. Instead, we suggest that the evolution of the interlayer electron-phonon coupling efficiency as a function of its thickness should also be considered. We developed a predictive model that takes both these effects into account. Combining this model to our experimental data, we calculated *g(T)* to range from 0.66 to 2.71 MW/m^3K depending on the substrate, which is close to values found in the literature. An exponential decay constant *k* of 2.73 was found to be a good value for all systems. Using these fitting parameters in our model allowed for a very accurate fit of our experimental data.

VI. ACKNOWLEDGEMENTS

The authors gratefully acknowledge the SNSF (Project No 200021_149290) for its financial support. Prof. O. Martin from the Nanophotonics and Metrology Laboratory (NAM, EPFL) is acknowledged for providing the laser source. Dr. A. Magrez from the iPhys platform (EPFL)

is acknowledged for his support with the Empyrean diffractometer and Dr. C. Monachon is acknowledged for having provided the code that enables TDTR data analysis.

REFERENCES

1. Rafailov, E. U., Cataluna, M. A., & Sibbett, W., Mode-locked quantum-dot lasers. *Nature photonics*, 1 (7) (2007) 395, DOI: 10.1038/nphoton.2007.120
2. Challener, W. A., Peng, C., Itagi, A. V., Karns, D., Peng, W., Peng, W., Yang, XM., Zhu, X., Gokemeijer N. J., Hsia, Y.-T., Ju, G., Rottmayer, R. E., Seigler, M. A., & Gage, E. C., Heat-assisted magnetic recording by a near-field transducer with efficient optical energy transfer. *Nature photonics*, 3(4) (2009) 220, DOI: 10.1038/nphoton.2009.26
3. Kemp, A. J., Valentine, G. J., Hopkins J.-M., Hastie, J. E., Smith, S. A., Calvez, S., Dawson, M. D., & Burns, D., Thermal management in vertical-external-cavity surface-emitting lasers: Finite-element analysis of a heatspreader approach. *IEEE Journal of Quantum Electronics*, 41(2) (2005) 148, DOI: 10.1109/JQE.2004.839706
4. Lyeo, H. K., & Cahill, D. G., Thermal conductance of interfaces between highly dissimilar materials. *Physical Review B*, 73(14) (2006) 144301, DOI: 10.1103/PhysRevB.73.144301
5. Monachon, C., Weber, L., & Dames, C., Thermal boundary conductance: A materials science perspective. *Annual Review of Materials Research*, 46 (2016) 433, DOI: 10.1146/annurev-matsci-070115-031719
6. Monachon, C., & Weber, L., Influence of diamond surface termination on thermal boundary conductance between Al and diamond. *Journal of Applied Physics*, 113(18) (2013) 183504, DOI: 10.1063/1.4804061
7. Losego, M. D., Grady, M. E., Sottos, N.R., Cahill, D. G., & Braun, P. V., Effects of chemical bonding on heat transport across interfaces. *Nature materials*, 11(6) (2012) 502, DOI: 10.1038/nmat3303
8. Collins, K. C., Chen, S., & Chen, G., Effects of surface chemistry on thermal conductance at aluminum–diamond interfaces. *Applied Physics Letters*, 97(8) (2010) 083102, DOI: 10.1063/1.3480413
9. Schmidt, A. J., Collins, K. C., Minnich, A. J., & Chen, G., Thermal conductance and phonon transmissivity of metal–graphite interfaces. *Journal of Applied Physics*, 107(10) (2010) 104907, DOI: 10.1063/1.3428464
10. Duda, J. C., Yang, C. Y., Foley, B. M., Cheaito, R., Medlin, D. L., Jones, R. E., & Hopkins, P. E., Influence of interfacial properties on thermal transport at gold: silicon contacts. *Applied Physics Letters*, 102(8) (2013) 081902, DOI: 10.1063/1.4793431
11. Wang, W., & Cahill, D. G., Limits to thermal transport in nanoscale metal bilayers due to weak electron-phonon coupling in Au and Cu. *Physical review letters*, 109(17) (2012) 175503, DOI: 10.1103/PhysRevLett.109.175503
12. Jeong, M., Freedman, J. P., Liang, H. J., Chow, C.-M., Sokalski, V. M., Bain, J. A., & Malen, J. A., Enhancement of thermal conductance at metal-dielectric interfaces using subnanometer metal adhesion layers. *Physical Review Applied*, 5(1) (2016) 014009, DOI: 10.1103/PhysRevApplied.5.014009
13. Monachon, C., Thermal boundary conductance between metals and dielectrics, (2013) DOI: 10.5075/epfl-thesis-5872
14. Björck, M., & Andersson, G., GenX: an extensible X-ray reflectivity refinement program utilizing differential evolution. *Journal of Applied Crystallography*, 40(6) (2007) 1174, DOI: 10.1107/S0021889807045086
15. Kang, K., Koh, Y. K., Chiritescu, C., Zheng, X., & Cahill, D. G., Two-tint pump-probe measurements using a femtosecond laser oscillator and sharp-edged optical filters. *Review of Scientific Instruments*, 79(11) (2008) 114901, DOI: 10.1063/1.3020759
16. Cahill, D. G., Analysis of heat flow in layered structures for time-domain thermoreflectance. *Review of scientific instruments*, 75(12) (2004) 5119, DOI: 10.1063/1.1819431
17. Haynes, W. M., CRC handbook of chemistry and physics. CRC press, (2014).
18. Stoner, R. J., & Maris, H. J., Kapitza conductance and heat flow between solids at temperatures from 50 to 300 K. *Physical Review B*, 48(22) (1993) 16373, DOI: 10.1103/PhysRevB.48.16373
19. Freedman, J. P., Yu, X., Davis, R. F., Gellman, & A. J., Malen, J. A., Thermal interface conductance across metal alloy–dielectric interfaces. *Physical Review B*, 93(3) (2016) 035309, DOI: 10.1103/PhysRevB.93.035309
20. Oh, D. W., Kim, S., Rogers, J. A., Cahill, D. G., & Sinha, S., Interfacial Thermal Conductance of Transfer-Printed Metal Films. *Advanced Materials*, 23(43) (2011) 5028, DOI: 10.1002/adma.201102994

21. Gundrum, B. C., Cahill, D. G., & Averback, R. S., Thermal conductance of metal-metal interfaces. Physical Review B, 72(24) (2005) 245426, DOI: 10.1103/PhysRevB.72.245426
22. Kittel, C., & McEuen, P., Introduction to solid-state physics (Vol. 8, pp. 323). New York: Wiley, (1996).
23. Hohlfeld, J., Wellershoff, S. S., Güdde, J., Conrad, U., Jähnke, V. & Matthias, E., Electron and lattice dynamics following optical excitation of metals. *Chemical Physics*, 251(1-3) (2000) 237, DOI: 10.1016/S0301-0104(99)00330-4
24. Lin, Z., Zhigilei, L. V., & Celli, V., Electron-phonon coupling and electron heat capacity of metals under conditions of strong electron-phonon non-equilibrium. *Physical Review B*, 77(7) (2008) 075133, DOI: 10.1103/PhysRevB.77.075133
25. Dederichs, P. H., Schober, H., & Sellmyer, D. J., Metals: Phonon states, electron states and Fermi surfaces, Landolt-Börnstein Group III Condensed Matter Vol. 13A (1981).
26. Martienssen, W., & Warlimont, H., Springer handbook of condensed matter and materials data. Springer Science & Business Media, (2006).